

**Fabrication of Functionalized Graphene Filled Carboxylated
Nitrile Rubber Nanocomposites as Flexible Dielectric
Material**

Journal:	<i>Materials Chemistry Frontiers</i>
Manuscript ID	QM-RES-04-2016-000025.R2
Article Type:	Research Article
Date Submitted by the Author:	29-Sep-2016
Complete List of Authors:	Manna, Rakesh; Indian Institute of Technology Kharagpur, Chemistry Srivastava, Suneel; Indian Institute of Technology, Kharagpur, Chemistry



Journal Name

ARTICLE

Fabrication of Functionalized Graphene Filled Carboxylated Nitrile Rubber Nanocomposites as Flexible Dielectric Material

Rakesh Manna and Suneel Kumar Srivastava*

Received 00th January 20xx,
Accepted 00th January 20xx

DOI: 10.1039/x0xx00000x

www.rsc.org/

Hexadecylamine (HDA) was used to covalently functionalize the graphite oxide followed by its reduction to form functionalized graphene nanosheet (GNS-HDA). Subsequently, GNS-HDA has been used as filler in fabricating carboxylated nitrile rubber (XNBR) nanocomposites via solution mixing. Mechanical measurements of XNBR/GNS-HDA-2 nanocomposite compared to neat XNBR exhibited 60 % improvement in tensile strength (TS), 62% improvement in elongation at break (EB) and 13 % reduction in Young's modulus (YM). Thermogravimetric studies demonstrate that incorporation of GNS-HDA in XNBR polymer matrix increases the thermal stability of composites with GNS-HDA loading. Further investigations show significant enhancement in dielectric constant of XNBR/GNS-HDA-2 (127.6) compared to neat XNBR (8.9) at 100 Hz. The corresponding value of the dielectric loss of the composite enhanced only ~ 2 times. Such enhanced TS, EB, reduced YM and dielectric constant while retaining low dielectric loss of XNBR/GNS-HDA enable for their possible applications as flexible dielectric material in electronic devices.

1. Introduction

Graphene is a two-dimensional material which is composed of several atomic sheets of sp^2 carbon atoms arranged in a hexagonal lattice. It remains one of the thinnest material compared to other allotropes of carbon (graphite, CNT, CF, fullerenes etc.). High specific surface area, high aspect ratio, superior high Young's modulus, fracture strength, and thermal conductivity of graphene make it an attractive material for many important applications.¹⁻³ Graphene has successfully been used as reinforcing filler in the polymer, exhibiting its outstanding structural, electrical, and mechanical properties. The low price and availability of the pristine graphite, followed by a simple methodology applied in the formation of graphene makes it one of the potential conductive filler in the polymers. However, poor dispersion of graphene in polymer matrix remains a major barrier and can be overcome by covalent and noncovalent functionalization.⁴⁻⁶ Further, low dielectric constant (less than 10) of most of the polymers restricts its direct application in many electrical fields. Therefore, it is desirable to find out ways to enhance the dielectric constant of polymer, while retaining low dielectric loss and good flexibility. Dielectric elastomers (DEs) are electroactive-polymers (EAPs), which have the ability to convert electrical energy to mechanical energy over a broad frequency range.^{7,8} The lightweight, low modulus, large strain, fast response, high energy density and high electromechanical coupling efficiency^{9,10} of DEs account for its application in artificial muscles, sensors, micro-air vehicles, flat-panel speakers, micro-robotics and responsive prosthetics.¹¹⁻¹⁴

In order to obtain a DEs in the application of high actuated strain and at the low electric field, a high value of electromechanical sensitivity, β (β =dielectric constant, k /elastic modulus, Y) is required. Accordingly, a high dielectric constant and low elastic modulus is the solution for this purpose. When conducting filler is incorporated in polymer matrices, k as well as Y values usually increase simultaneously.

The dielectric constant of the polymer can be enhanced by incorporating high dielectric constant ceramic materials such as $BaTiO_3$, TiO_2 . But high amount of ceramic material (50 vol.%) is required to enhance the desired dielectric constant, resulting enhancement in elastic modulus, lowering in flexibility and poor processability, which narrow down the applications of DEs. Alternatively, DEs can also be fabricated through percolative composite by incorporating conducting fillers such as graphene sheet, and carbon nanotube.¹⁵⁻¹⁸ The choice of graphene in such work is also guided by its easy synthesis from natural graphite compared to the carbon nanotube. The dispersion of covalent¹⁹⁻²³ and non-covalent modified²⁴⁻²⁹ graphene and filler-polymer interfacial interaction account for its reinforcing ability, especially at low filler loading. Interestingly, the dielectric constant of such polymer composite increases abruptly near the percolation threshold¹⁸. When the percolation threshold is reached, an undesirable enhancement of dielectric loss of composites is also inevitable⁴. The existing literature also highlights inferior extensibility of these polymer nanocomposites.^{30,31} In view of this, several rubbers filled with graphene oxide or graphene has been investigated as DE materials. poly(isobutylene-co-isoprene)/reduced graphene oxide nanocomposites was prepared by solution blending method at 5 wt% loading. It introduces the dielectric property over a broad frequency range and at a different temperature. The result shows that dielectric constant at room temperature for reduced graphene oxide nanocomposites increases 10 times (29 at 10^{-2} Hz) when it is compared with expanded graphite composite (2.9).³² Al-Hartomy et al³³ studied dielectric

Inorganic Materials and Nanocomposites Laboratory
Department of Chemistry,
Indian Institute of Technology, Kharagpur-721302, India
E-mail: sunil111954@yahoo.co.uk

Electronic Supplementary Information (ESI) available: Stress-strain plots, comparative table of Young's Modulus

and microwave properties of graphene nanoplatelets (1 to 5 phr) /carbon black (50 phr) filled natural rubber composites in the 1-12 GHz frequency range. Graphene oxide-based dielectric elastomer composite material exhibiting high dielectric constant and electric breakdown strength and low dielectric loss.^{4,34-39} Potts et al.³⁴ fabricated NR/2wt% reduced graphene oxide (RGO) nanocomposites by co-coagulating latex composites followed by mixing in two roll mill and observed reduction in elongation at break by 50%. It is also reported that increased dispersion level and interaction between rubber chain and filler materials render the dissipation of external stress throughout the polymer matrix. The dissipation of external stress can occur through alignment and slippage of rubber chains, which is adsorbed on the surface of nanofiller.³⁵ Poly(dimethyl) siloxane embedded with 2 wt % of thermally expanded graphene sheet showed an increment in k from 2.7 to 23 at the frequency of 10 Hz.⁴ The low increment in dielectric constant than expected could be ascribed to the poor dispersion and restacking of graphene sheets. In another interesting work, Jiang et al.,¹⁴ Prepared 5 wt % loaded hyper branched aromatic polyamide functionalized graphene sheets (GS-HBA) into the TPU matrix and achieved the enhancement in k value to 850 at 1000 Hz. However, the low dielectric loss is retained (<1.5) due to the suppression of leakage current by hyperbranched aromatic polyamide functional group. Noncovalent-modified graphene (3%) polyurethane nanocomposite showed the dielectric constant of 350, the dielectric loss of 0.20 and loss modulus of 200 MPa at room temperature in 1 kHz.³⁶ According to Ning et al.,³⁷ poly(dopamine) (PDA) coated GO (GO-PDA) was assembled around carboxylated nitrile rubber (XNBR) latex showed that dielectric loss and the elastic modulus decrease, and the breakdown strength increases with increasing the thickness of PDA shell. Tian et al.³⁸ reported that carboxylated nitrile rubber (XNBR)/graphene oxide nanosheet encapsulated carbon sphere (GON-CNS) nanocomposites by latex. The compounding dielectric composites exhibited low dielectric loss and improved breakdown strength and actuated strain at a low electric field facilitating the wide application of dielectric elastomer. Another work involved formation of dielectric composite prepared by using the combined strategy of encapsulating of graphene oxide nanosheets (GONS) on XNBR latex particles and the in situ thermal reduction in GONS at a moderate temperature.³⁹ The corresponding nanocomposites exhibited high dielectric constant, low dielectric loss and low percolation threshold. The available literature also suggested that high aspect ratio and low content of graphene³⁷⁻³⁹ are enough to enhance k value compared to ceramic dielectric filler,^{7,8} and retains low elastic modulus and better processability. It is to be noted that carboxylation of the butadiene-acrylonitrile latex confers colloidal stability.⁴⁰ In addition, XNBR latex is also stabilised with at least one external surface-active agent.⁴⁰ However, drawback of latex stabilization during storage, mixing, and processing are determined by time, temperature, phase separation, pH drift, shear in mixing etc.⁴¹ Therefore, it would be interesting to use raw rubbers as alternatives in order to overcome all these undesirable hurdles in fabrication of flexible dielectric elastomeric nanocomposites. However, no significant advances have been achieved in fabricating mechanically improved and thermally enhanced XNBR/graphene dielectric material directly from XNBR rubber and overcome undesirable hurdles in fabrication imposed by corresponding latex.

Motivated by this, we focused our work on functionalization of graphene nanosheets (GNS) surface by hexadecyl amine (HDA). It is anticipated that such modification of graphene could also reduce the dielectric loss by preventing the direct current conductance and

enhance the compatibility of functionalized reduced graphene oxide with the polymer matrix. Further, low elastic modulus of the composite could overall lead their application as flexible dielectric material. The choice of carboxylated nitrile rubber (XNBR) in our work is mainly guided by the presence of strong polar carboxyl and cyano groups, which could form a strong adhesion between GNS-HDA and XNBR. Finally, these XNBR/GNS-HDA nanocomposites have been studied for their thermal stability, mechanical and dielectric properties.

2. Experimental

2.1 Materials

XNBR (Krynac® X 740, LANXESS) and graphite Micro-850 were procured from Germany and Asbury Graphite Mills, INC., Asbury, NJ. respectively. HDA (98%), ethanol, dicumyl peroxide (DCP), sodium nitrate (NaNO_3) were supplied by SRL (Mumbai), Hercules (USA) and S. D. Fine Chemicals (India) respectively. Potassium permanganate (KMnO_4), concentrated sulfuric acid (H_2SO_4), hydrogen peroxide (H_2O_2), and hydrazine hydrate (N_2H_4) were purchased from Merck, India. Tetrahydrofuran (THF) was obtained from RFCL Limited, New Delhi.

2.2 Preparation of graphene oxide

GO was prepared by the modified Hummers' method reported earlier.⁴² According to this, graphite (500 mg) along with sodium nitrate (250 mg) were taken in a beaker, containing 30 ml concentrated H_2SO_4 , followed by addition of 1.5 g KMnO_4 in stirring condition for 30 min. The resulting mixture was diluted with deionized water and then 10 ml of H_2O_2 was added to this. As a result, the color of the solution turned to brilliant yellow, indicating the formation of fully exfoliated graphene oxide. Finally, the product free from metal ions was obtained by washing it several times with dilute HCl followed by deionized water to remove the free acid.

2.3 Preparation of hexadecyl amine functionalized graphene

Graphene oxide (200 mg) nanosheets prepared earlier by Hummers' method were dispersed in 30 ml of water by sonication for 30 min. Subsequently, HDA modified graphene was prepared based on the idea referred from earlier work.^{43,44} Accordingly, HDA (300 mg) was dissolved in ethanol (60 ml) followed by heating and cooling. This cooled solution of HDA was added to the dispersion of graphite oxide in water prepared earlier with sonication continuing for 30 min. The resultant mixture was subsequently refluxed at 100 °C in presence of hydroquinone (400 mg) for 24 hours. The formed solid product (GNS-HDA) was centrifuged followed by washing with ethanol and drying at 65 °C in vacuum for 24 h. The prepared GNS-HDA is as indicated by its dispersion in organic nonpolar solvent (tetrahydrofuran, cyclohexane, toluene, and ethanol etc)

2.4 Preparation of GNS-HDA/XNBR composites

XNBR/GNS-HDA nanocomposites were prepared by solution mixing method. Initially, GNS-HDA nano filler (0, 0.5, 1, 1.5, 2 phr) were dispersed in THF with the assistance of ultrasonicator for 5 min. Accordingly, 5 g of XNBR was dissolved in 50 mL THF in a 100 cc beaker. In another beaker, a required amount of GNS-HDA nano filler was dispersed in THF under ultrasonic treatment for 5 min.

Following this, it was added to XNBR solution at room temperature and magnetically stirred for ½ an hour, followed by the addition of 2 phr DCP. The stirring was continued for another 6 h. Finally, the solution was cast in glass petri dish to evaporate the solvent, THF, at room temperature. Finally, cast films were cured at 160 °C for 10 min, according to the cure time obtained from oscillating disc rheometer analysis (ODR). In a similar manner, XNBR composites filled with 0.5, 1.0, 1.5 and 2 phr of GNS-HDA were also fabricated. The obtained sheets were taken for further characterization and application.

2.5 Characterization

The structure of GNS-HDA had been analyzed by Fourier transform infrared spectroscopy (FTIR) on PerkinElmer RXI FTIR spectrometer, USA in the frequency range of 400-4000 cm^{-1} . The crystalline/amorphous nature of GNS-HDA was obtained by carrying out X-ray diffraction analysis on Bruker D8, Advanced X-ray diffractometer with $\text{Cu K}\alpha$ ($\lambda = 0.1542$ nm) radiation in the 2θ range of 5° to 80° and at a scan rate of $10^\circ/\text{min}$. Morphology of samples was analyzed by TEM using JEOL2100 microscope at a voltage of 200 keV. The sample preparation for TEM observation was carried out by cutting the composite film with an ultramicrotome into thin sections of 100 nm thickness with a diamond knife and the sample was collected on 200-mesh copper grids. The morphology of the tensile fractured surface of samples was studied by Novanano SEM 430 scanning electron microscope (Germany). Atomic force microscopy (AFM) measurement was carried out on a Veeco Multimode V scanning probe microscope in tapping mode. Samples for AFM images of GNS-HDA and GNS were prepared by spin coating on a mica surface using 0.1 mg/ml dispersion in THF. Thermal stability of samples was carried out on a TGA Q5000 instrument in the temperature range of 60-600 °C at a heating rate of $10^\circ\text{C}/\text{min}$ in nitrogen gas purging. Differential scanning calorimetry (DSC) measurement of the sample was recorded on TA instruments Q-20 from -50°C to room temperature. Dielectric properties were performed using QuadTech 7600 precision LCR meter in the frequency range 10 Hz to 1 MHz.

3. Results and discussion

3.1 Structure and morphology of GNS-HDA

Fourier transform infrared (FTIR) spectra of HDA and GNS-HDA are displayed in Figure 1. It is clearly evident that two asymmetric bands appeared at about 2849 cm^{-1} and 2917 cm^{-1} in HDA as well as the presence of an amine group ($-\text{NH}_2$) in GNS-HDA, clearly signifying functionalization of graphene nanosheet by HDA. Further, the appearance of the carbonyl stretching vibration at 1644 cm^{-1} established the formation of a linkage between the reduced graphite nanosheet and HDA. It is known that graphene oxide (GO) consists of hydroxyl ($-\text{OH}$) and epoxy groups lying above and below the basal planes and the carboxyl groups ($-\text{COOH}$) bound to the edges.³⁷ Therefore, it is anticipated that functionalization of GO takes place via covalent bonding between the $-\text{NH}_2$ (HDA) and $-\text{COOH}$ (GO) groups as proposed in Scheme 1.

Figure 2 shows XRD patterns of GNS and GNS-HDA. It is noted that (002) diffraction peak appeared in GNS at $\sim 24^\circ$, corresponding to d-spacing of 0.34 nm. However, (002) diffraction peak of GNS-HDA appeared at 21.5° ($d_{002} = 0.41$ nm). These findings further strengthened our contention based on FTIR about the attachment of amine group (HDA) on the graphene nano sheet. In order to

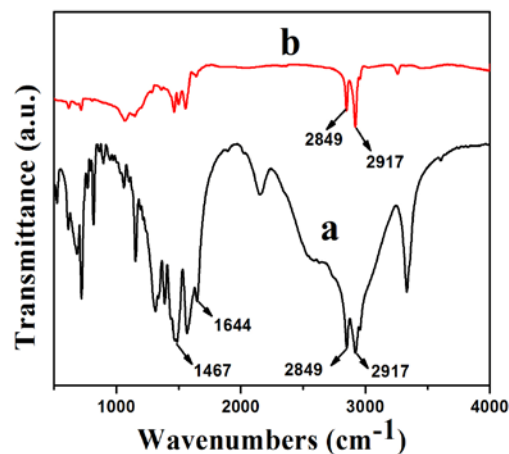


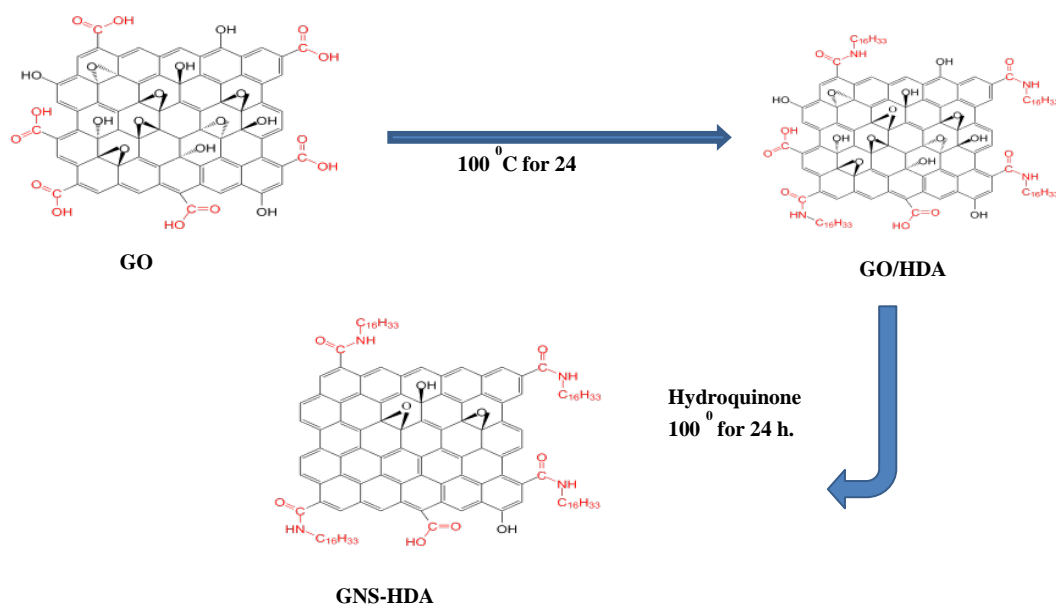
Figure 1: FTIR Spectra of (a) GNS-HDA and (b) HDA

further validation, AFM analysis of GNS and GNS-HDA were recorded in tapping mode and displayed in Figure 3. The multilayers with broad distribution in thickness and size are clearly evident from this. The height of GNS layers is found to be ~ 1 nm and less than that of graphite oxide due to the expulsion of different oxygen functionalities ($>\text{C}=\text{O}$, $-\text{COOH}$, $-\text{OH}$, $-\text{O}-$).

However, HDA functionalized graphene sheets exhibited relatively higher thickness (~ 2 nm).⁵ Our findings are also in agreement with AFM studies reported on individually dispersed graphene and rhodamine B noncovalently modified graphene exhibiting a thickness of about 1 and 1.6 nm respectively.⁴⁵

The morphology of GNS and GNS-HDA has been studied by FESEM and TEM analysis and corresponding findings are displayed in Figure 4. It is clearly evident that GNS-HDA exists as aggregated, thin crumpled nanosheets and largely associated with each other. TEM image of GNS-HDA showed the appearance of flat and rippled morphology. The presence of light gray color in this image corresponds to the formation of dispersed GNS-HDA thin layer, while darker regions indicated the stacking of GNS-HDA layers.

Thermal stability behavior of GO, GNS, and GNS-HDA has been investigated in the temperature range of 60-600 °C under nitrogen atmosphere and corresponding findings are displayed in Figure 5. The initial weight loss ($\sim 12\%$) in GO between 60° to 130°C can be ascribed to the adsorbed water. At further higher temperature, TG shows a weight loss of 56 % in the range of 130 - 325°C due to pyrolysis of hydroxyl, carbonyl, epoxy, and carboxylic acid groups in GO. After 325°C no significant weight loss is noticed due to the expulsion of oxygen functionalities in GO. It is also noted that GNS and GNS-HDA both are thermally stable up to 195°C . This suggested that neither GNS nor GNS-HDA is sensitive towards moisture adsorption. This could be ascribed to the enhanced hydrophobic nature of GNS-HDA achieved by effective functionalization of HDA on the graphene surface. At higher temperature, GNS undergoes significantly low weight loss of $\sim 5\%$ due to incomplete reduction of the remaining oxygen functionalities in GO. In contrast, degradation of GNS-HDA takes place much faster and achieve weight loss of $\sim 80\%$ (495°C). This is attributed to complete degradation of hexadecylamine due to functionalization of GNS. However, the possibility of a fraction of HDA adsorbed on the surface of graphene also cannot be ruled out.³⁵ Room temperature dispersion stability of GNS-HDA and GNS has been investigated for THF (10 mg/ml) for about 1-month duration by recording its digitized image. Figure 6 shows that



Scheme 1 Chemical functionalization of HDA on graphene sheet

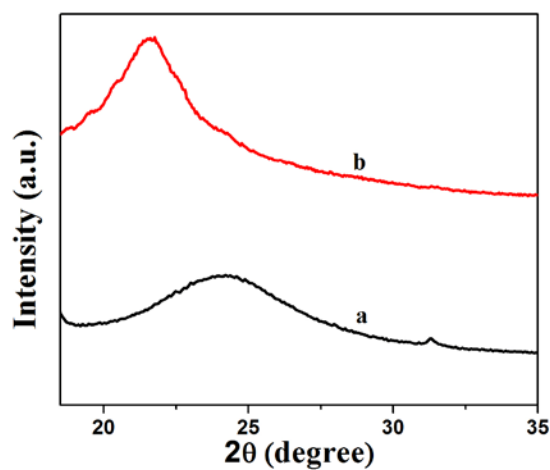


Figure 2: XRD patterns of (a) GNS and (b) GNS-HDA

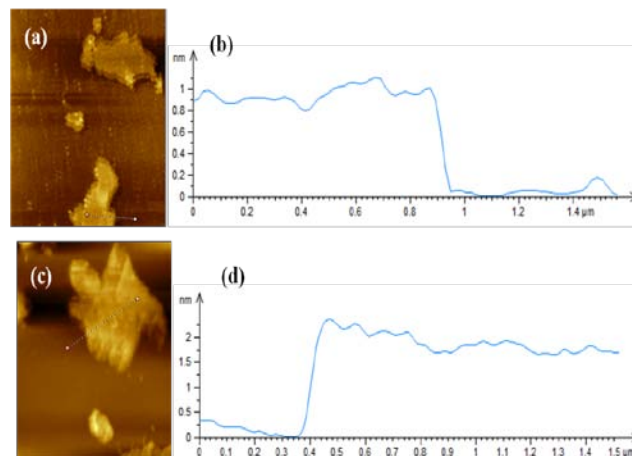


Figure 3: AFM image of (a) GNS, (b) height profile of GNS, (c) AFM image of GNS-HDA, (d) height profile of GNS-HDA.

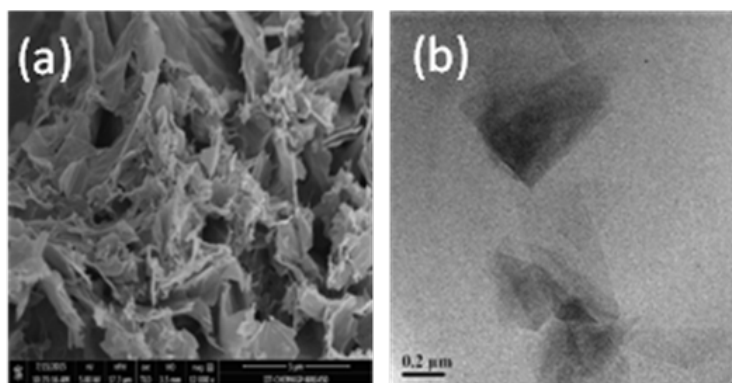


Figure 4: (a) FESEM and (b) TEM images of GNS-HDA

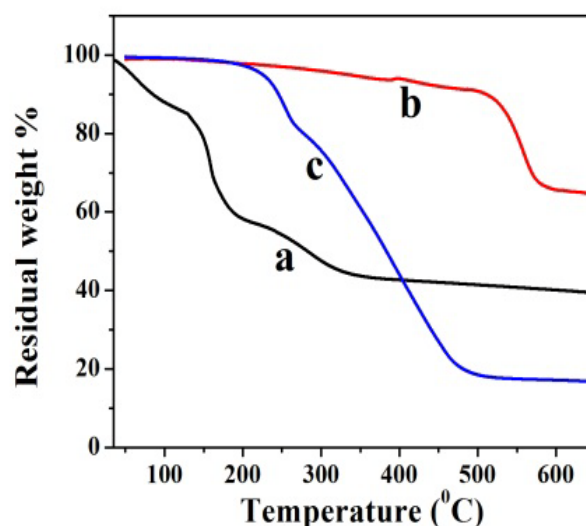


Figure 5: TGA of (a) GO, (b) GNS, and (c) GNS-HDA

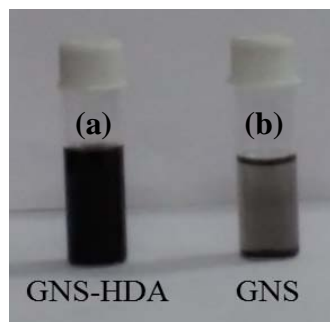


Figure 6: Digital picture of dispersion stability of (a) GNS-HDA and (b) GNS

chemically functionalized GNS-HDA has significantly higher dispersion stability in THF compared to GNS.

3.2 Structure and morphology of GNS-HDA/XNBR composites

Figure 7 shows XRD patterns of XNBR and its 0.5, 1, 1.5 and 2 phr GNS-HDA loaded nanocomposites. It is noted that crystalline and a broad diffraction peak of GNS-HDA ($2\theta=21.50$) completely disappeared in all nanocomposites. Such observations demonstrated possible exfoliation of GNS-HDA in the XNBR matrix.^{39,46} In order to further validate this, HRTEM analysis of XNBR/GNS-HDA composites have also been carried out and findings are displayed in Figure 8. It clearly shows wrinkled and folded sheets of GNS-HDA exhibit good dispersion in XNBR matrix. This is in all probability due to compatibility between GNS-HDA and XNBR matrix and account for the significantly enhanced properties of XNBR/GNS-HDA nanocomposites.

3.3 TGA of XNBR and composites

There are various studies which demonstrate that the incorporation of graphene sheet into the polymer matrix enhances the thermal stability of composites under nitrogen atmospheric condition.⁴⁷ Figure 9 shows thermal stability behavior of neat XNBR, 0.5, 1, 1.5, and 2 phr GNS-HDA filled XNBR in nitrogen atmosphere and corresponding thermal data referring to thermal degradation temperature at 10% wt. loss (T_{10}) are 388, 392, 393, 393, and 394 °C for 0, 0.5, 1, 1.5, and 2 phr GNS-HDA loading respectively. These findings clearly demonstrate that incorporation of GNS-HDA in XNBR polymer matrix increases the thermal stability of composites with GNS-HDA loading. However, XNBR/GNS-HDA (0.5 wt%) shows significant improvement in thermal stability compared to neat XNBR. Such enhancement in thermal stability of XNBR/GNS-HDA nanocomposites is ascribed to the high aspect ratio of graphene and complete exfoliation of GNS-HDA in XNBR polymer matrix. As a result, emission of volatile decomposed gaseous products and supply of oxygen from the surface to the bulk is hindered due to an effective barrier effect of GNS-HDA.⁴⁷

3.4 DSC

Chemically modified graphene loaded polymers usually show enhancement in glass transition temperature (T_g).^{48,49} This is attributed to close proximity of embedded nanoparticles in the polymer macromolecules, which restricts the chain mobility of polymer chains at interface.⁴⁸⁻⁵⁰ In contrast, DSC analysis of neat XNBR and its GNS-HDA filled nanocomposites in Figure 10 showed that T_g of XNBR decreased from -18 °C in all XNBR/GNS-HDA

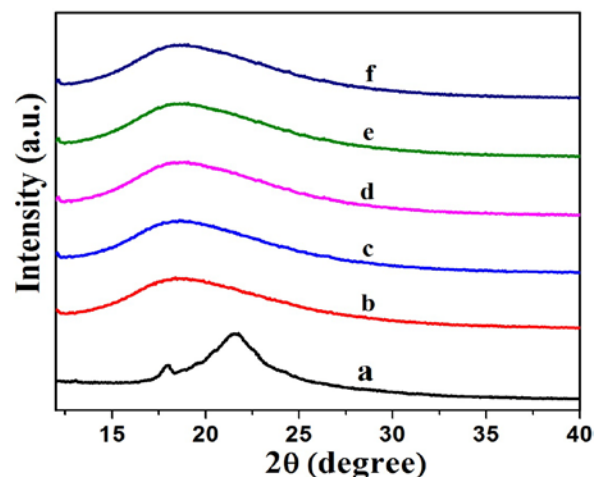


Figure 7: XRD spectra of (a) GNS-HDA, and (b) neat XNBR, (c) 0.5 phr, (d) 1 phr, (e) 1.5 phr, (f) 2 phr GNS-HDA filled XNBR composites

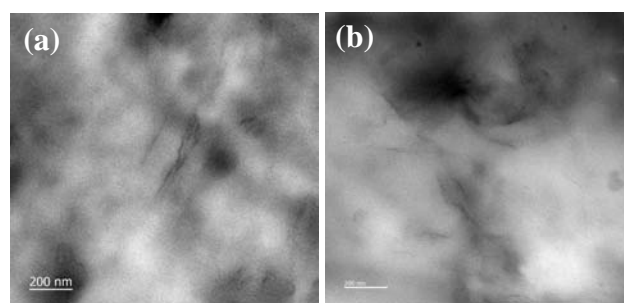


Figure 8: HRTEM of (a) 1 phr (b) 1.5 phr, GNS-HDA filled XNBR composites.

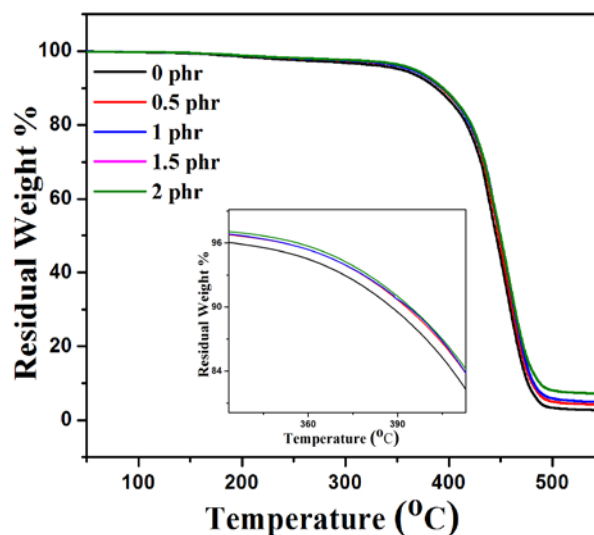


Figure 9: TGA curve of XNBR and various GNS-HDA/XNBR

nanocomposites. The maximum decrease in T_g of -20 °C is attained in 2 phr GNS-HDA loaded XNBR. This could be ascribed to enhanced chain mobility due to the presence of free surfaces and repulsive interfaces in XNBR/GNS-HDA nanocomposites.^{51,52} Alternatively, lowering of T_g in XNBR/GNS-HDA nanocomposites could be attributed to the plasticization effect⁵³ or free volume existing at the polymer surface interface.⁵⁴

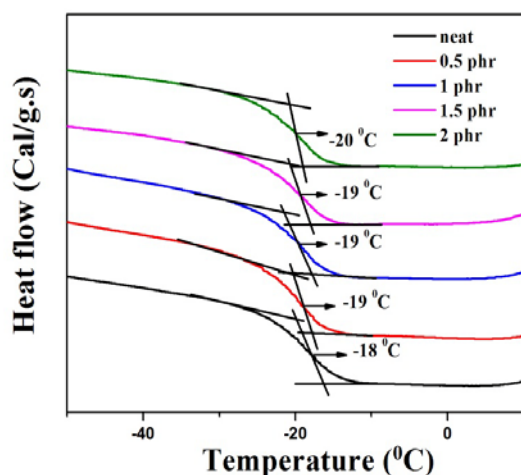


Figure 10: DSC curve of XNBR and various GNS-HDA/XNBR.

3.5 Mechanical properties

The reinforcing effect of GNS-HDA on mechanical properties of neat XNBR has also been investigated. Tensile strength (TS), elongation at break (EB), toughness (W), and Young's modulus (YM) data has been generated from stress-strain plot (ESI1) and displayed in Figure 11, 12, and 13, respectively. It is noted that TS of neat XNBR (2.9 MPa) increases with the incorporation of filler loading and attained maximum improvements (4.63MPa) in 2phr GNS-HDA loaded XNBR. The variation in EB also shows improvement in 1, 1.5 and 2 phr filled GNS-HDA in XNBR compared to neat XNBR. It is also noted that EB of neat XNBR (227%) is increased substantially to 365% in 2 phr loaded GNS-HDA in XNBR. The toughness of the GNS-HDA/XNBR composites also increases significantly with filler loading. It is well anticipated that higher dispersion of nanomaterial in polymer matrix renders better performance of its nanocomposites. Such enhancement in mechanical properties of XNBR/GNS-HDA nanocomposites could be attributed to the interfacial interaction between GNS-HDA and XNBR matrix and effective load transfer from filler to the polymer matrix.^{46,50} Alternatively, the role of molecular level dispersion of GNS-HDA and its wrinkled shape leading to mechanical interlocking and transmitting the applied stress to XNBR also cannot be ruled out.⁵¹ In addition, crumpled GNS-HDA adds some extra reinforcement at high elongation when it is stretched, which attributes the enhancement of toughness and elongation at break.⁵¹ Figure 14 shows FESEM images of the tensile fracture surface of XNBR and its GNS-HDA filled nanocomposites. It demonstrates that XNBR exhibits smooth surface in contrast to the corresponding GNS-HDA composites, exhibiting divergence on the surface. The extent of divergence increases with increase in GNS-HDA loading in XNBR matrix. The YM defines the slope of the curve in the elastic region. It is inferred from Figure 13 that YM of composites is reduced remarkably in GNS-HDA incorporated XNBR. This clearly indicates the reduced stiffness and enhanced flexibility of fabricated XNBR/GNS-HDA nanocomposites. It is also noted that 2 phr of GNS-HDA loaded XNBR showed a maximum decrease of about 13 % in YM compared to neat XNBR. Such findings are found to be considerably superior compared to that reported in TRG/XNBR nanocomposites earlier.³⁹ In most of the graphene polymer composites, the modulus enhances with the incorporation of filler loading,^{38,39} which is contrary to our study (ESI2). The increase in toughness and decrease in YM suggest that GNS-HDA existing as almost single sheet adopting a wrinkled morphology that imparts a

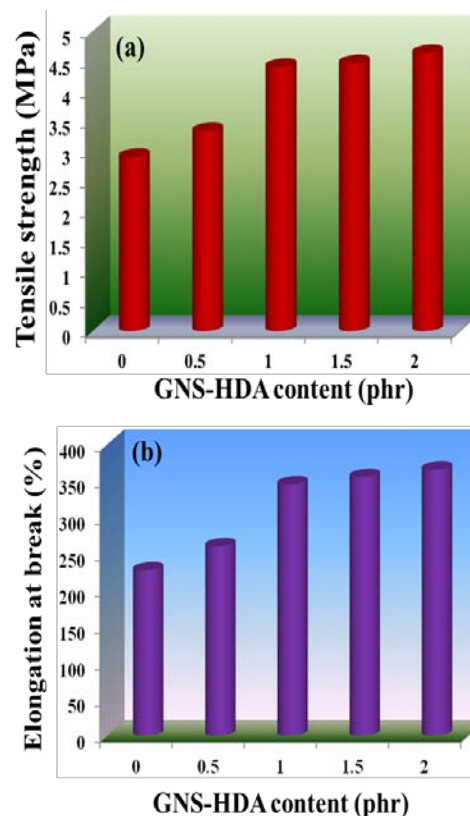


Figure 11: (a) Tensile strength and (b) Elongation at break of neat XNBR and various GNS-HDA/XNBR composite

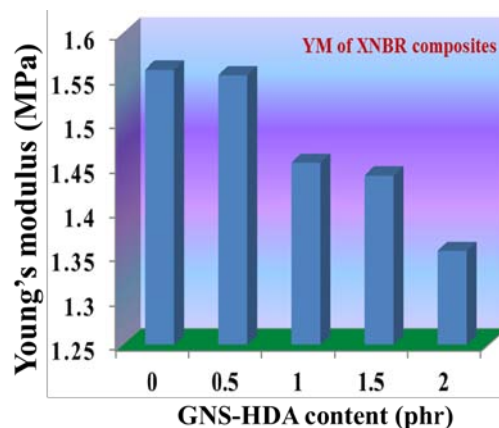


Figure 12: Young's modulus of neat XNBR and various GNS-HDA/XNBR composites

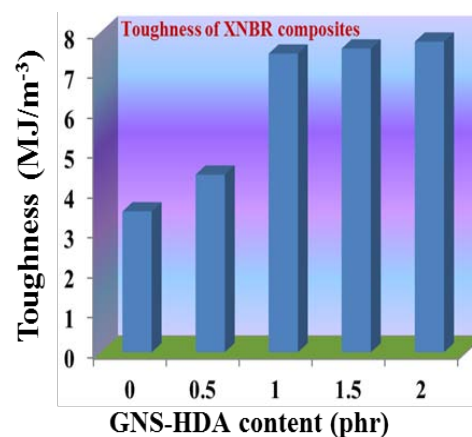


Figure 13: Toughness of neat XNBR and various GNS-HDA/XNBR composites

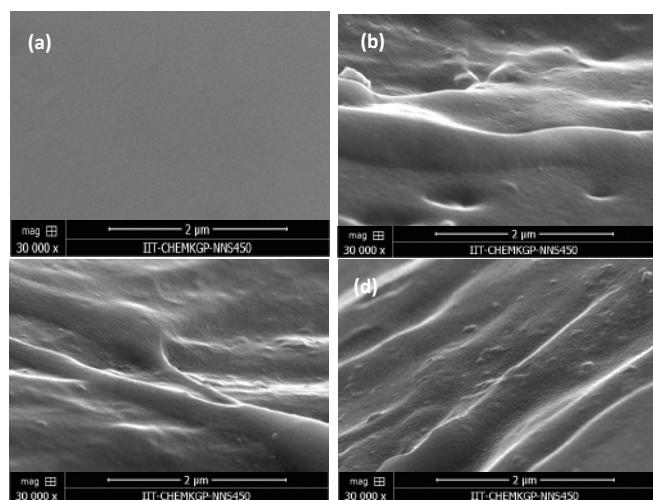


Figure 14: FESEM images of tensile fracture surface of (a) neat XNBR, (b) 1 phr, (c) 1.5 phr, and (d) 2 phr GNS-HDA loading.

measure of entropic and rubber like elasticity itself. Further, low modulus of wrinkled GNS-HDA single sheets and high compatibility between XNBR and GNS-HDA can also account for the lowering of modulus in its XNBR nanocomposites.

3.6 Dielectric properties

Figure 15 and 16 show variation of dielectric permittivity (k) and dielectric loss of neat XNBR and its GNS-HDA composites as a function of frequency ($\log f$). It is inevitable that dielectric permittivity decreases with increasing frequency for XNBR and its GNS-HDA composites. Such strong frequency dependence of dielectric permittivity can be attributed to the interfacial polarization effect between the GNS-HDA and XNBR (Maxwell-Wagner-Sillars effect).³⁹ The findings, based on dielectric constant and dielectric loss data of XNBR and its GNS-HDA composites at 100 Hz along with the values reported on other elastomers are presented in Table 1. HDA filled XNBR nanocomposite increases nearly 15 fold, whereas dielectric loss increases to 2 fold only compared to neat XNBR. It is also evident from Figure 15 that dielectric permittivity of GNS-HDA/XNBR composites is relatively higher in the low frequency range ($\log f$: 1-3) followed by a significant decrease at higher frequency region. In all probability, accumulation of charge between GNS-HDA and XNBR at the interfaces in the low frequency region accounts for higher dielectric permittivity value of composites. At higher frequency, interfacial polarization lags behind the frequency of electrical field frequency. Dielectric permittivity of composites increases with the increase in filler loading. Further, it may be interesting to mention that presence of conductive GNS-HDA filler (electrode) in XNBR (insulating) form the micro capacitor network.¹⁴ However, successful functionalization also plays a crucial role in the enhancement of dielectric permittivity. Alternatively, there is a possibility that successful functionalization of graphene sheet can reduce its restacking tendency.³⁵ This, in turn, is likely to enhance a number of microcapacitor in the polymer matrix and ultimately accounts for its higher dielectric permittivity value.¹⁴ In polymer composite, the dielectric loss generally occurs due to dipolar loss, conduction loss, and interfacial polarization loss. In graphene polymer composite, conduction loss may occur due to leakage current through direct current conduction through graphene. Figure

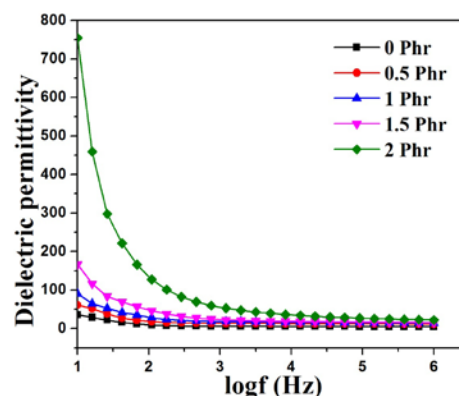


Figure 15: Dielectric constant vs. log (frequency) for neat XNBR and various GNS-HDA/XNBR composites.

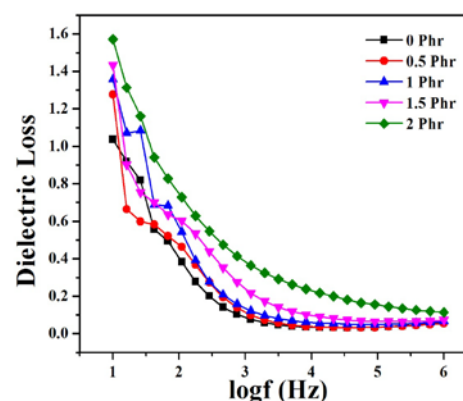


Figure 16: Dielectric loss vs. log (frequency) for neat XNBR and various GNS-HDA/XNBR composites

Table 1: Dielectric properties of XNBR and composites

GNS-HDA (phr)	Dielectric permittivity @100 Hz	Dielectric loss @100 Hz
0	8.9	0.38
0.5	17.8	0.46
1	28	0.54
1.5	46.3	0.60
2	127.6	0.73

16 shows a variation of dielectric loss as a function of the frequency of XNBR and its nanocomposites; corresponding data at 100 Hz are recorded in Table 1. It is noted that dielectric loss of XNBR (0.38) increases with GNS-HDA loading and attain a maximum value of 0.73 in 2 phr loaded composites at 100 Hz. Such negligible enhancement in dielectric losses can arise due to the interruption of π -conjugation in GNS-HDA, which seems to be due to covalent functionalization. This leads to a reduction in the direct current conductance in graphene sheet and hinder enhancement, if any, in dielectric loss in case of its XNBR nanocomposites. It may be noted that GNS-HDA/XNBR achieved dielectric permittivity (127 at 100 Hz) compared to that reported in TRG/XNBR (2211 at 100 Hz),³⁹ PDA-GO/XNBR (250 at 100 Hz),³⁷ PEDOT:PSS-RGO@PU (350 at 1000 Hz)³⁶ and GO@CNS/XNBR (650).³⁸ However, dielectric loss values of GNS-HDA/XNBR (0.8 at 100 Hz) were found to be comparable with TRG/XNBR (0.6 at 100 Hz),³⁹ PDA-GO/XNBR (1.2 at 100 Hz),³⁷

PEDOT:PSS-RGO@PU (~0.2 at 1 kHz)⁴⁵ and GO@CNS/XNBR (1.7 at 100 Hz),⁴⁶ systems.

4. Conclusion

A simple facile solution mixing method has successfully been used in developing highly dispersed HDA functionalized graphene nanocomposites of XNBR and characterized. The mechanical properties at a various loading of HDA functionalized graphene showed efficient load transfer. As a consequence, XNBR/GNS-HDA-2 exhibited significant improvement in tensile strength (60 %) and elongation at break (62 %). Furthermore, measurement of dielectric properties indicated a maximum enhancement in dielectric constant by 15 times (100 Hz), whereas dielectric loss is increased by 2 fold only. The thermal study showed that reduction in glass transition temperature (T_g) of XNBR/GNS-HDA-2 is responsible for the reduction in elastic modulus. This is in all probability due to the lower elastic modulus of wrinkled and single sheet graphene produced by hexadecyl amine functionalization compare to XNBR. Such reduction in elastic modulus including enhanced tensile strength/dielectric permittivity and very low dielectric loss makes these composites useful for their applications as flexible dielectric material in various electronic devices.

5. Acknowledgements

S. K. Srivastava and Rakesh Manna gratefully acknowledge DRDO, India and IIT Kharagpur for grants to R. Manna for perusing research.

6. Notes and References

- 1 K. S. Novoselov, A. K. Geim, S. V. Morozov, D. Jiang, Y. Zhang, S. V. Dubonos, I. V. Grigorieva, A. A. Firsov, *Science*, 2004, **306**, 666.
- 2 K. S. Novoselov, A. K. Geim, S. V. Morozov, D. Jiang, M. I. Katsnelson, I. V. Grigorieva, S. V. Dubonos, A. A. Firsov, *Nature*, 2005, **438**, 197.
- 3 Y. Zhang, Y. Tan, H. L. Stormer, P. Kim, *Nature*, 2005, **438**, 201.
- 4 L. J. Romasanta, M. Hernandez, M. A. Lopez-Manchado and R. Verdejo, *Nanoscale Res. Lett.*, 2011, **6**, 205.
- 5 Y. Luo, P. Zhao, Q. Yang, D. He, L. Kong, Z. Peng, *Compos. Sci. Technol.*, 2014, **100**, 143.
- 6 S. Mo, L. Peng, C. Yuan, C. Zhao, W. Tang, C. Ma, J. Shen, W. Yang, Y. Yu, Y. Min and A. J. Epstein, *RSC Adv.*, 2015, **5**, 97738
- 7 Y. Song, Y. Shen, H. Liu, Y. Lin, M. Li and C. Nan, *J. Mater. Chem.*, 2012, **22**, 16491.
- 8 R. Shankar, T. K. Ghosh, R. J. Spontak, *Soft Matter*, 2007, **3**, 1116.
- 9 Y. Jang, T. Hirai, *Soft Matter*, 2011, **7**, 10818.
- 10 R. Palakodeti, M.R. Kessler, *Mater. Lett.*, 2006, **60**, 3437.
- 11 Y. Rao, C. P. Wong, *J. Appl. Polym. Sci.*, 2004, **92**, 2228.
- 12 S. M. Ha, W. Yuan, Q. Pei, R. Pelrine, S. Stanford, *Adv. Mater.*, 2006, **18**, 887.
- 13 R. Pelrine, R. Kornbluh, Q. Pei, J. Joseph, *Science*, 2000, **287**, 836.
- 14 C. Wu, X. Huang, G. Wang, X. Wu, K. Yang, S. Lib, P. Jiang, *J. Mater. Chem.*, 2012, **22**, 7010.
- 15 X. Zhang, G. Wang, W. Cao, Y. Wei, M. Caob, L. Guo, *RSC Adv.*, 2014, **4**, 19594.
- 16 J. Shang, Y. Zhang, L. Yu, B. Shen, F. Lv, P. K. Chu, *Mater. Chem. Phys.*, 2012, **134**, 867
- 17 Z.M. Dang, L. Wang, Y. Yin, Q. Zhang, and Q. Q. Lei, *Adv. Mater.*, 2007, **19**, 852.
- 18 J. Shang, Y. Zhang, L. Yu, B. Shen, F. Lv, P. K. Chu, *Mater. Chem. Phys.*, 2012, **134**, 867
- 19 M. Cano, U. Khan, T. Sainsbury, A. O'Neill, Z. Wang, I. T. MCGovern, W. K. Maser, A. M. Benito, J. N. Coleman, *Carbon*, 2013, **52**, 363.
- 20 M. Fang, Z. Zhang, J. Li, H. Zhang, H. Lu, Y. Yang, *J. Mater. Chem.*, 2010, **20**, 9635.
- 21 K. Manna, S. K. Srivastava, and Vikas Mittal, *J. Phys. Chem. C*, 2016, **120**, 17011.
- 22 Z. Li, R. Wang, R. J. Young, L. Deng, F. Yang, L. Hao, W. Jiao, W. Liu, *Polymer*, 2013, **54**, 6437.
- 23 S. Hou, S. Su, M. L. Kasner, P. Shah, K. Patel, C. J. Madarang, *Chem. Phys. Lett.*, 2010, **501**, 68.
- 24 Y. Xu, H. Bai, G. Lu, C. Li, G. Shi, *J. Am. Chem. Soc.*, 2008, **130**, 5856.
- 25 H. Bai, Y. Xu, L. Zhao, C. Li, G. Shi, *Chem. Commun.*, 2009, **13**, 1667.
- 26 R. Liao, Z. Tang, Y. Lei, B. Guo, *J. Phys. Chem. C*, 2011, **115**, 20740.
- 27 Y. Lei, Z. Tang, R. Liao, B. Guo, *Green Chem.*, 2011, **13**, 1655.
- 28 Z. Tang, C. Zeng, Y. Lei, B. Guo, L. Zhang, D. Jia, *J. Mater. Chem.*, 2011, **21**, 17111.
- 29 Z. Tang, Y. Lei, B. Guo, L. Zhang, D. Jia, *Polymer*, 2012, **53**, 673.
- 30 M. Hernandez, M. d. M. Bernal, R. Verdejo, T. A. Ezquerro, M. A. Lopez-Manchado, *Compos. Sci. Technol.*, 2012, **73**, 40.
- 31 J. R. Potts, O. Shankar, S. Murali, L. Du, R. S. Ruoff, *Compos. Sci. Technol.*, 2013, **74**, 166.
- 32 S. K. Kumar, M. Castro, A. Saiter, L. Delbreilh, J. F. Feller, S. Thomas, Y. Grohens, *Materials letters*, 2013, **96**, 109.
- 33 O. A. Al-Hartomy, A. A. Al-Ghamdi, F. Al-Salamy, N. Dishovsky, R. Shtarkova, V. Iliev, F. El-Tantawy, *International Journal of Materials and Chemistry*, 2012, **2**, 116
- 34 J. R. Potts, O. Shankar, S. Murali, L. Du, R. S. Ruoff, *Compos. Sci. Technol.*, 2013, **13**, **74**, 166.
- 35 X. Liu, D. Sun, L. Wang, and B. Guo, *Ind. Eng. Chem. Res.*, 2013, **52**, 14592.
- 36 T. Chen, J. Qiu, K. Zhu, J. Li, J. Wang, S. Lib and X. Wang, *RSC Adv.*, 2014, **4**, 64061
- 37 N. Ning, Q. Ma, S. Liu, M. Tian, L. Zhang, and T. Nishi, *ACS Appl. Mater. Interfaces*, 2015, **7**, 10755.
- 38 M. Tian, Q. Ma, X. Li, L. Zhang, T. Nishic, N. Ning, *J. Mater. Chem. A*, 2014, **2**, 11144.
- 39 M. Tian, J. Zhang, L. Zhang, S. Liu, X. Zan, T. Nishi, N. Ning, *J. Colloid Interface Sci.*, 2014, **430**, 249.
- 40 H. M. Ghazaly, and P.P. La, *J. Rubb. Res.*, **4(2)**, 88.
- 41 O. H. Nautiyal, DOI: 10.5923/j.ajps.20120202.03.
- 42 L. Shahriary, A. A. Athawale, *IJREEE*, 2014, **2**, 2348.
- 43 J. Jang, V. H. Pham, S. H. Hur, J. S. Chung, *J. Colloid Interface Sci.*, 2014, **424**, 62.
- 44 G. Wang, X. Shen, B. Wang, J. Yao, J. Park, *Carbon*, 2009, **47**, 1359.
- 45 Z. Tang, Y. Lei, B. Guo, L. Zhang, D. Jia, *Polymer*, 2012, **53**, 673.
- 46 Y. Wan, L. Tang, L. Gong, D. Yan, Y. Li, L. Wu, J. Jiang, G. Lai, *Carbon*, 2014, **69**, 467.
- 47 T. Kuila, S. Bose, A. K. Mishra, P. Khanra, N. H. Kim, J. H. Lee, *Polym. Test.*, 2012, **31**, 31.
- 48 D.R. Paul, L.M. Robeson, *Polymer*, 2008, **49**, 3187.
- 49 T. Ramanathan, A. A. Abdala, S. Stankovich, D. A. Dikin, M. H. Alonso, R. D. Piner, D. H. Adamson, H. C. Schniepp, X. Chen, R. S. Ruoff, S. T. Nguyen, I. A. Aksay, R. K. P. Homme and L. C. Brinson, *Nat. Nanotechnol.*, 2008, **3**, 327.

Journal Name

ARTICLE

50 R. D. Priestley, C. J. Ellison, L. J. Broadbelt, J. M. Torkelson, *Science*, 2005, **309**, 456.

51 Jeffrey R. Potts, Daniel R. Dreyer, Christopher W. Bielawski, Rodney S. Ruoffa, *Polymer*, 2011, **52**, 5.

52 C.J. Ellison, J.M. Torkelson, *Nat Mater*, 2003, **2**, 695.

53 M. Pluta, J.K. Jeszka, G. Boiteux, *Eur. Polym. J.*, 2007, **43**, 2819.

54 P. Rittigstein, J. M. Torkelson, DOI: 10.1002/polb.20925